Journal of Electrical Engineering, Vol. 74, No. 4, 2023, pp. 246-255

sciendo

PAPER

Inhomogeneous HfO_2 layer growth at atomic layer deposition

Aarne Kasikov[1], Aivar Tarre[1], Guillermo Vinuesa[2]

Thin HfO_2 films atomic layer deposited from hafnium alkyl amide and oxygen plasma were analysed using spectroscopic ellipsometry and X-ray reflectivity. Low refractive index of the material for samples with less than 30 nm thickness marks the index inhomogeneity at the first stage of growth. The transition from rising density to a more stable growth takes place at about 10 to 25 nm film thickness. HfO_2 films used for resistive switching experiments demonstrate either clockwise or counterclockwise behaviour depending on the film thickness. The reason for this may be the disruption of the conductive filament at different metal-insulator interfaces, which could be favoured by several mechanisms.

Keywords: hafnium thin films, spectroscopic ellipsometry, growth inhomogeneity, atomic layer deposition, packing density, resistive switching, filament formation.

1. Introduction

Hafnium oxide (HfO_2) is a material highly used in its pure form or mixed with other dielectrics in optics as an optical coating due to its high laser-induced defect threshold [1,2], and in electronics as the dielectric [3]. There have been the attempts to use it as resistive switching material for random access memories [4,5], explore the ferroelectric properties of HfO_2 orthorhombic or monoclinic phase [6] and to use of the films for gas sensing [7]. The thin films based on hafnium dioxide have been produced by atomic layer deposition (ALD) [6,8,9], plasma-enhanced ALD [1,10], sputtering [11], reactive electron gun evaporation [12], reactive molecular beam epitaxy [13] or by ion-assisted deposition [14]. For HfO_2 films deposited by ALD the 3D growth due to the onset of crystallization have been shown at the first stages of growth with the coalescence of the 3D islands afterwards [15]. Crystallization of the material has also been shown to cause a transversal negative optical inhomogeneity for films with thickness over 100 nm [7,12,16].

2. Instrumentation

The HfO_2 films were grown on Si(100) substrates in the R200 Advanced (Picosun, Finland) atomic layer deposition reactor using tetrakis(ethylmethylamino)hafnium (TEMAH, 99%, Strem) and O_2 plasma as precursors. The growth sequence was 0.3-8-15-8 s (for TEMAH pulse – N_2 purge – O_2/Ar plasma pulse – N_2 purge, respectively). The films were grown by 50 - 500 ALD cycles at the temperatures ranging from 150 to 400 °C.

The films were analysed *ex situ* using spectroscopic ellipsometry (SE), X-ray reflectivity (XRR) and X-ray diffraction. Ellipsometry measurements were performed at 75° incidence angle using GES-5E ellipsometer (Semilab, Hungary) with microspot option. The ellipsometric spectra were analysed using WinElliII and SEA (Semilab) programs. The X-ray measurements were performed using an X-ray diffractometer SmartLab (Rigaku, Japan).

Tauc-Lorentz and Cauchy dispersion models were used to obtain the film parameters. For thinnest films, Tauc-Lorentz dispersion failed due to heaping of the parameters. As the detailed analysis of the film optical properties for films with thickness of tens of nanometres is complicated, the simplest Cauchy dispersion model was used in analysis for all the films and a function of refractive index dependence on thickness found. The low refractive index of the films pointed on defectness (see below) of the thinner HfO_2 films, so one term for absorption was included in the model.

Electrical characterization of the films was carried out by means of a Keithley 4200-SCS semiconductor parameter analyser and a probe station. DC voltage was applied to the top electrode, while the bottom one remained grounded in all cases. Current-voltage (I-V) measurements were made to observe the resistive switching effect shown by some of the devices by applying voltage sweeps.

[1] Institute of Physics, University of Tartu, W. Ostwaldi 1, 50411 Tartu, Estonia
[2] Department of Electronics, University of Valladolid, Paseo de Belén 15, 47011 Valladolid, Spain
[1] aarnek@ut.ee

https://doi.org/10.2478/jee-2023-0031, Print (till 2015) ISSN 1335-3632, On-line ISSN 1339-309X
© This is an open access article licensed under the Creative Commons Attribution-NonCommercial-NoDerivs License (http: //creativecommons.org/licenses/by-nc-nd/4.0/).

3. Experimental

3.1 Ellipsometry results

The SE refractive index values obtained in the attempt to characterize our thinner films were abnormally low, reaching the values below 1.5 for the thinnest samples grown using 55 ALD cycles. This means that we have not yet reached the stable growth mode at this point. For illustration of the situation, the arbitrary refractive index dependence of some material on film thickness is presented in Fig. 1. If a refractive index of the film rises with thickness and the ellipsometric parameters of the film are obtained in homogeneous layer approximation (the vertical and horizontal lines creating a rectangle characterizing the optical thickness of the film by its calculated thickness and refractive index), the refractive index result should be lower than the refractive index on the upper interface of the film and higher than that at the lower interface (in contact with the substrate).

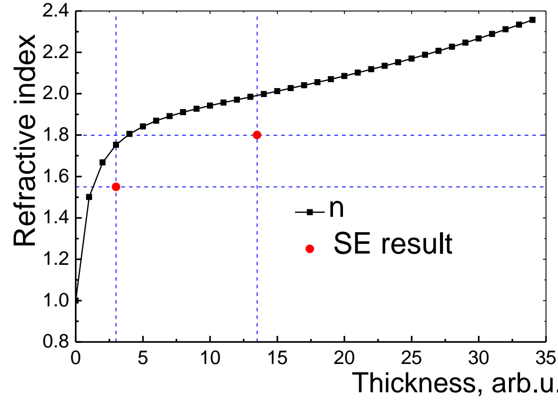

Fig. 1. A model refractive index dependence on thickness for inhomogeneous film. The points mark the ellipsometry results for calculation in homogeneous approximation.

Using XRR we saw the film density values for 500 cycles of ALD growth being dependent on the deposition temperature (Fig. 2). If the material maximum density is taken from monoclinic phase cell parameters [17] as 10.14 g/cm^3 and HfO_2 maximum refractive index [18,19] at 633 nm as $n = 2.1$, we can estimate the refractive index for this wavelength at each temperature using Bruggeman effective media approximation

$$f\frac{n_1^2-n^2}{n_1^2+2n^2}+(1-f)\frac{n_2^2-n^2}{n_2^2+2n^2}=0. \tag{1}$$

Here, f is the relative density of the material, n_1 and n_2 the refractive indices of the material and the air, $n_2 = 1$. We propose that the refractive index n_1 corresponds to the material with main part of the material deposited in stable mode.

Figure 3 presents the results of the modelling of HfO_2 films for 633 nm wavelength depending on temperature. For thicker samples the results obtained using Tauc-Lorentz and Cauchy dispersion models coincide quite well while for 55 cycle films no reliable results were obtained using Tauc-Lorentz dispersion. For 110 and 500 cycle samples the Bruggeman EMA modelling results proceeding from [18] maximal refractive index value is also presented. We see that the refractive indices calculated from XRR densities do not differ much. Including the refractive index dependencies into the model for thicker films gave only the hints of refractive index rising with film thickness but not quantitative information.

Now, we present the refractive index results at 633 nm from SE calculations dependent on film thickness (Fig. 4). If we take a logarithm of the cycle number (or logarithm of the calculated film thickness value), the results could be quite well approximated by a linear function. It means that the refractive index for a mean material is given through the integral of film optical thickness (Fig. 1) as

$$\frac{1}{X}\int_0^X n(x)dx = a\ln(X)+b. \tag{2}$$

Here, the left side of the equation corresponds to the mean refractive index of the film with thickness X. Moving film thickness (defined either in growth cycles or in physical thickness values) on the right side, we get

$$\int_0^X n(x)dx = a\,X\,ln(X)+b\,X \tag{3}$$

and after differentiation, the local refractive index will approximately be presented as

$$n(x) = (a + b) + a\,ln(x) \quad (4)$$

After the ellipsometric analysis of the films, this procedure was performed for each temperature, with cycle number or a film thickness as an argument, and for different absorption terms used ($1/\lambda$, $1/\lambda^2$ or $1/\lambda^3$). In all the cases the correlation value R^2 between the measured and modelled spectra was about 0.999, so there was no reason to use more elaborate dispersion model. The maximum value for parameter uncertainty was 25% for regression constant a and 7.5% for regression constant b.

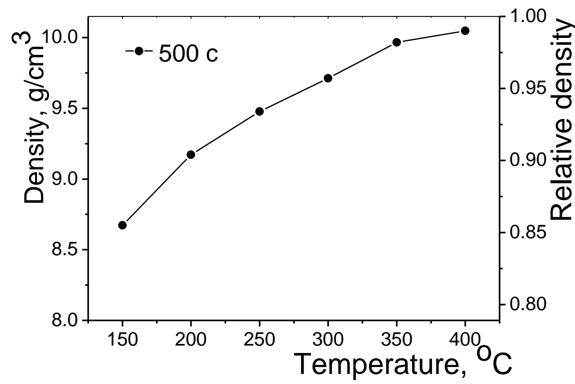

Fig. 2. Thick films (500 ALD cycles) density values from XRR allow the estimation of their relative density compared to single crystal data. From here, the approximate final refractive index values for a film depending on growth temperature can be calculated.

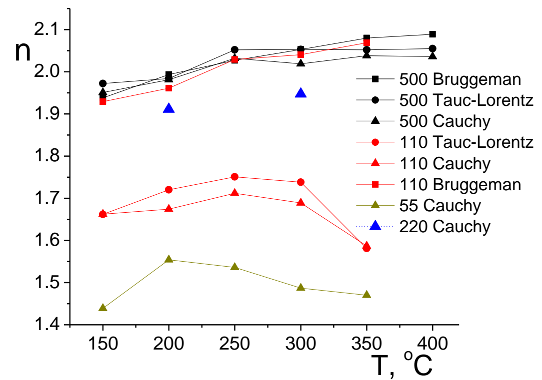

Fig. 3. Refractive index values at 633 nm for the HfO_2 films with different number of ALD cycles calculated using Bruggeman EMA approximation or SE modelling with either Tauc-Lorentz or Cauchy dispersion models.

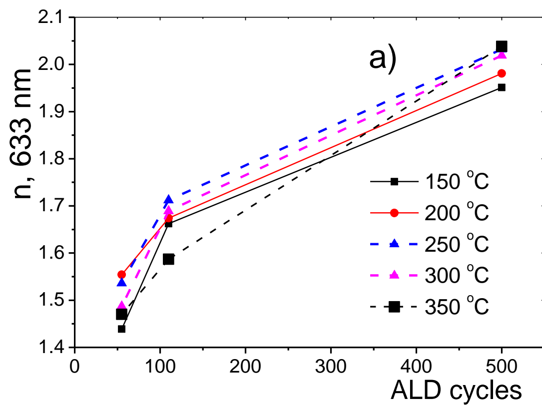

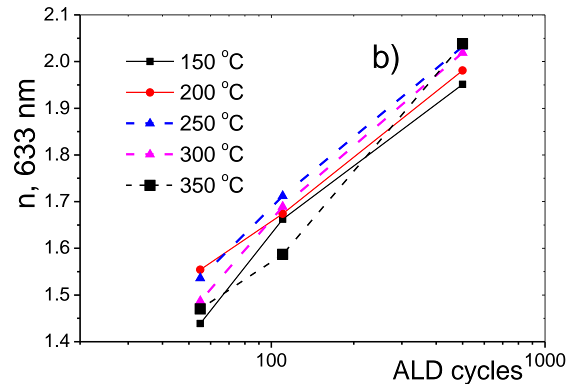

Fig. 4. Refractive index dependence on the number of ALD cycles. Linear (a) and semilogarithmic (b) dependencies on the cycle number.

The semilogarithmic graph allowed to guesstimate the refractive index values at the film thickness points and the thickness values where the stable growth (taken here as the local refractive index equalling thick material index) is achieved. It happens at about 100 to 250 growth cycles (approximately 15 to 25 nm film thickness) from 150 to 350 °C growth temperature (Fig. 5).

The available objects deposited using 220 ALD cycles at 200 and 300 °C allow us to give more physical presentation of refractive index behaviour. Fig. 6 shows stabilizing of the films mean refractive index taking place between 110 (second thickness point) and 500 (fourth point) cycles of growth. So, we have two possible regressions on a figure, either for samples from 55 to 220 cycles (reg1), or for samples 55 to 500 cycles (reg2) as it is obtained for other process temperatures where the 220 cycle samples were not available. A similar picture is obtained for 300 °C (not shown).

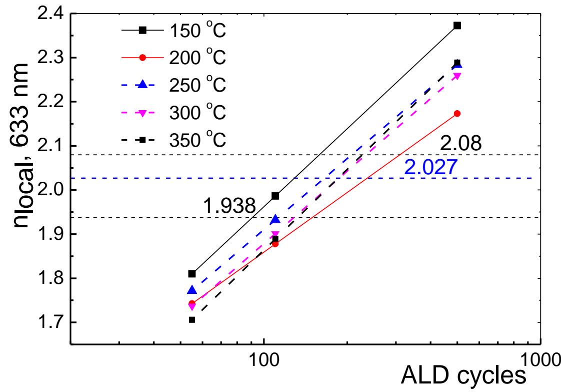

Fig. 5. Calculated film local refractive index values at a border with air obtained from linear regression. The horizontal lines show the refractive index calculated from XRR data for 500 cycles films grown at 150, 250 and 350 °C.

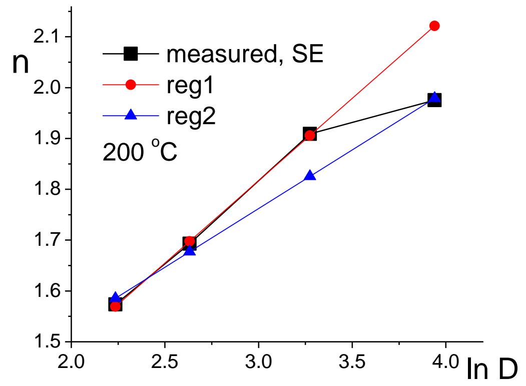

Fig. 6. Film ellipsometric refractive index behaviour dependent on thickness natural logarithm for 200 °C growth. Different linear regressions can be drawn with different choice of measurement points.

Figure 7 presents the modelled dependence of the refractive index on thickness for a film grown at 200 °C. The local refractive index rises faster and reaches the index value we proposed for a stable film (500 cycles), while the (mean) index calculated from the ellipsometric data in our homogeneous film approximation continues to grow due to lower refractive index values at the first stages of the growth. Using reg1 calculated up to 220 cycles growth (about 27 nm), we get near stable growth from 12 nm thickness on, the reg2 dependence used for a full set of samples beforehand would stabilize later. Both models eventually fail at higher thickness values.

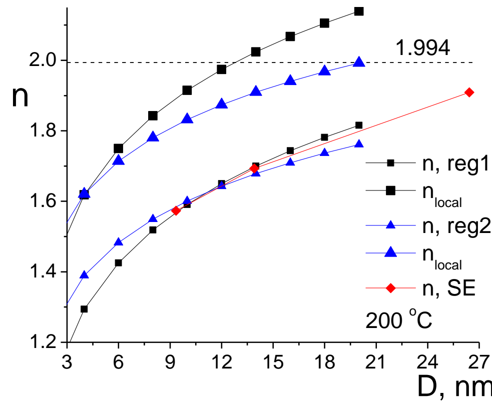

Fig. 7. The estimated local refractive index dependences reach the value of the maximum refractive index for a thick film obtained from XRR. Calculations with two linear regression dependencies using the refractive index values from ellipsometry. Data for 200 °C.

To check the reliability of our modelling we can compare the optical parameter results obtained with different arguments. The measured refractive index values for 250 °C deposition temperature using different absorption functions are presented in Fig. 8a. We see that except for thinnest sample, the refractive index values do not depend much on absorption model.

On the other side, the absorption index values at 355 nm for 150 °C deposition temperature (Fig. 8b) can be under doubt as they behave not as a smooth function on thickness and have clearly lower values than the samples grown at other temperatures. All the power functions give similar absorption dependencies, while for all temperatures over 200 °C it is better to use the higher power functions to describe the absorption index (Fig. 8d).

We suppose the reason may be the onset of crystallization already at lower thicknesses for films grown at higher temperatures while at 150 and 200 °C the material remains amorphous over full range of thicknesses and we can speak about porous network of hafnia only.

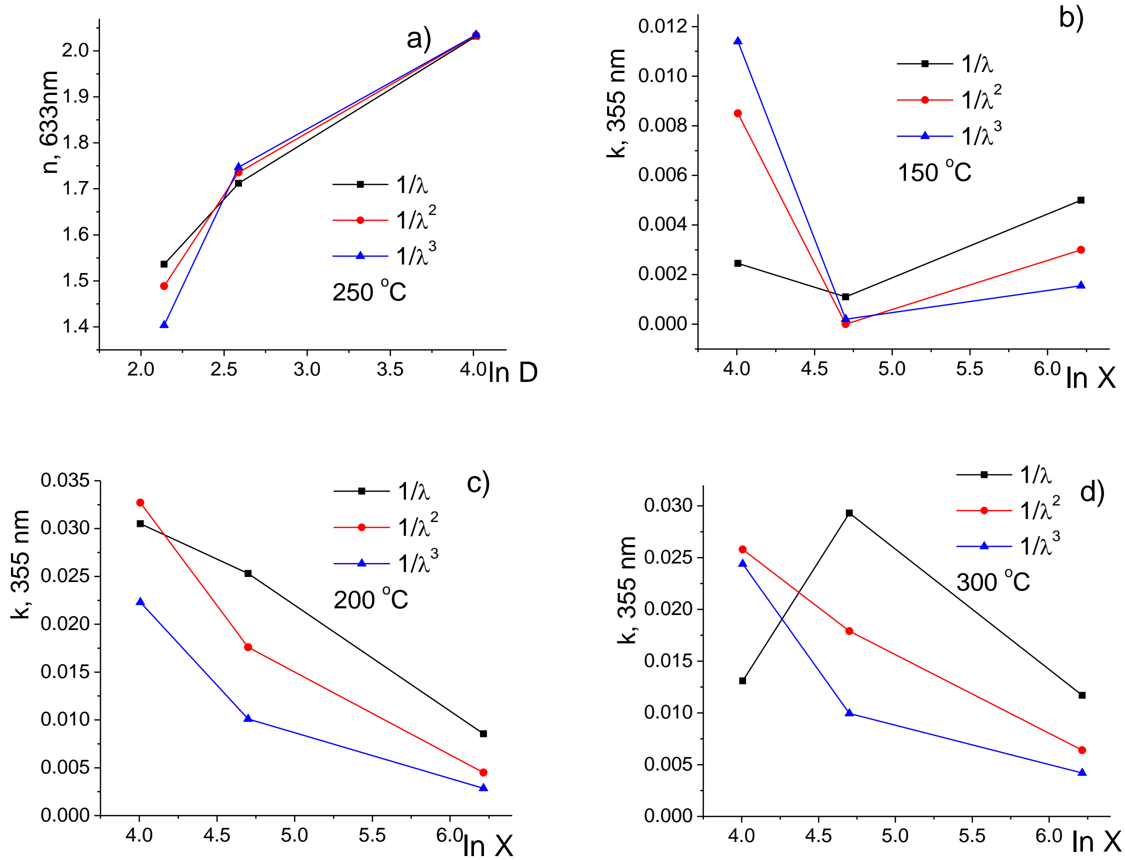

Fig. 8. The refractive index dependence on film thickness at 633 nm (a); the absorption index dependence on ALD growth cycles at 355 nm for different power functions used to describe the absorption term (b-d). The growth temperatures are marked on graphs.

3.2 Resistive switching

Devices with no electrochemically active metals as electrodes and based on HfO_2 are known to deliver the resistive switching mechanism due to the valence-change mechanism (VCM) [20]. In VCM based samples, applying an electric field leads oxygen vacancies to form conductive filaments (CFs) through the dielectric, short-circuiting the metal electrodes and decreasing the sample's resistivity (SET process). Another electric field disrupts these filaments, increasing again the resistivity (RESET process), but never as if the sample was pristine. Both the SET and RESET processes will take place only after the CFs are formed for the first time after the electroforming process, which usually requires a much larger applied voltage than the SET, as well as a current compliance in order not to irreversibly damage the sample [21,22].

Two of the 200 ºC ALD grown Ti/TiN/Ti/HfO_2/Pt/Cr metal-insulator-metal devices (HfO_2 thickness about 8.5 nm and 14 nm according to SE) have shown excellent bipolar resistive switching capabilities (BRS). However, as can be seen in Figs. 9 (a) and (b), a dependence on film thickness was observed, with the thinner sample delivering counter-clockwise resistive switching (CCW RS) and the thicker film showing clockwise (CW) RS [5]. The approximate local refractive indices for 50 and 100-cycles films were about 1.65 and 2.0 on upper interface found using the procedure presented above, accordingly, and the estimated packing densities for these cases would be 0.61 and 0.90. This change in resistive switching polarity has also been observed for the same ALD grown samples but with inverted metal electrodes (Pt/Cr/HfO_2 (8.5 and 14 nm)/Ti/TiN (Figs. 9 (c) and (d)). This proves that the RS polarity dependence on thickness is repetitive.

The explanation behind the different resistive switching behaviours was hypothesized to be due to the filament breaking at different metal-insulator interface, as the previous studies suggest [23,24]. The CCW RS is well studied and reported in several other studies, it is believed to be caused by the Ti cap behaving as an oxygen reservoir, thus creating an oxygen-vacancy rich zone near the top electrode. This allows the formation of a CF with its thicker part near the Ti cap [24]. Nevertheless, the CW RS has also been reported by other authors in a previous work that studied similar samples as the ones presented here [25]. In this study, the polarity change occurred in a 5.5 nm HfO_2 thick layer that showed both CW and CCW RS. The change in polarity was based

on a current overshoot provoked by parasitic capacitances discharge, that leads to further ion migration after the electroforming process. Indeed, for the samples presented here, the thicker sample showed a much higher electroforming voltage (-8 V) than its thinner counterpart (4 V), which could favour the mechanism proposed by Brivio *et al* [25]. Furthermore, both the studies conducted by Vinuesa and Brivio [5,25], respectively, observed an anomalous peak that indicates the two mechanisms (CW and CCW) competing in the 14 nm sample. The 14 nm sample has also shown unipolar resistive switching (URS) (Fig. 10), and it cannot be ruled out that the URS is competing with the CW or CCW RS [26], leading to the polarity change with the HfO_2 layer thickness increase. This explanation is plausible, as URS has been observed in MIM stacks with the same layer configuration as the one presented here [27].

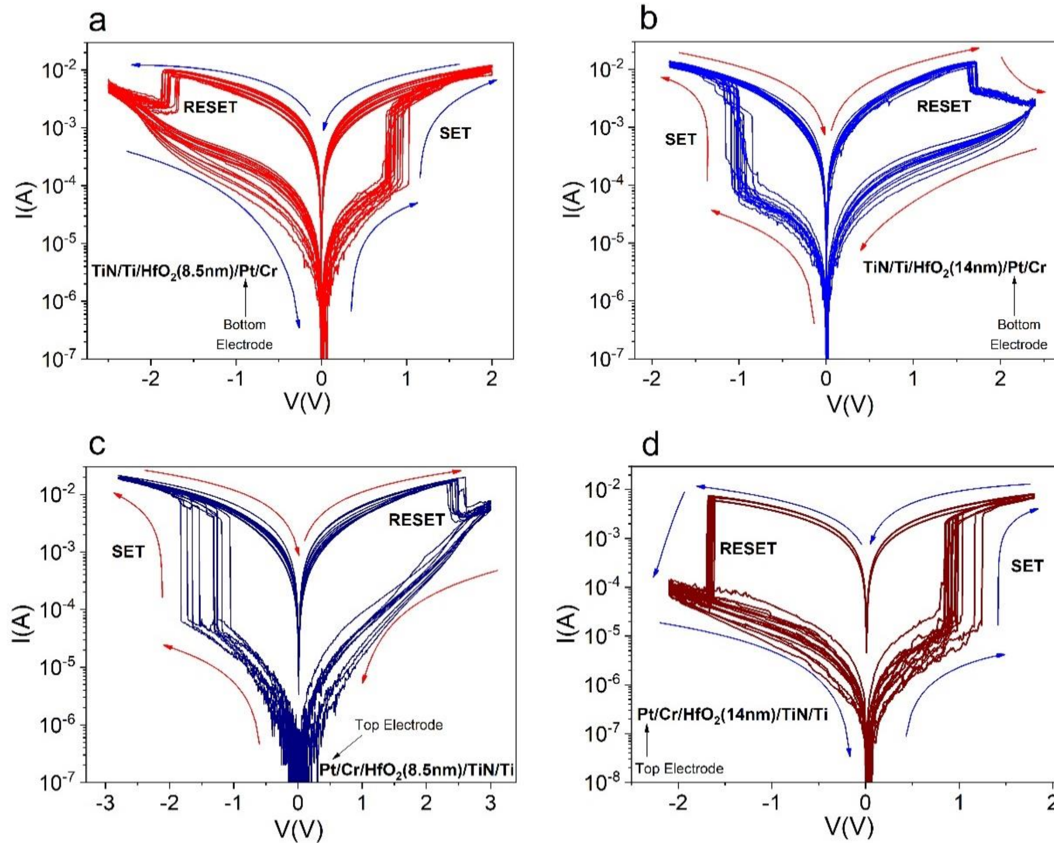

Fig. 9. I-V curves of the $TiN/Ti/HfO_2/Pt/Cr$ with HfO_2 layers of 8.5 nm (a) and 14 nm (b). I-V curves of the $Pt/Cr/HfO_2/TiN/Ti$ with HfO_2 layers of 8.5 nm (c) and 14 nm (d).

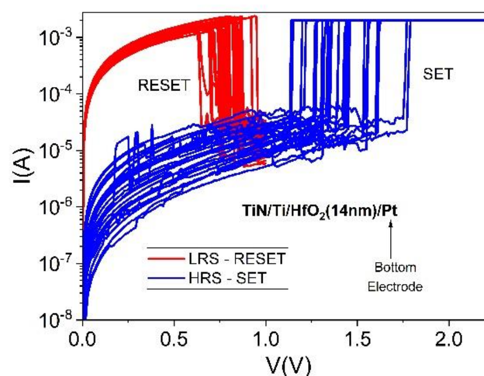

Fig. 10. I-V curves of the unipolar resistive switching exhibited by the $TiN/Ti/HfO_2/Pt$ sample with a 14 nm thick HfO_2 layer.

Moreover, because the Ti cap has the same thickness in both devices, but the HfO_2 layer is 5 nm thicker, the titanium layer is no longer thicker than the HfO_2, and thus, could not form a large enough oxygen vacancy rich zone near the Ti/HfO_2 interface This could also lead to the polarity change of the 14 nm thick device (Fig. 11). The measured packing densities may also be the reason behind the filament disruption occurring at different metal - insulator interfaces, as the thinner sample has also a lower packing density in the HfO_2/Ti interface. This is significant because this interface composition changes as the device goes through the switching in sub-sequent cycles, and metal-insulator interactions are of critical importance in VCM devices [28].

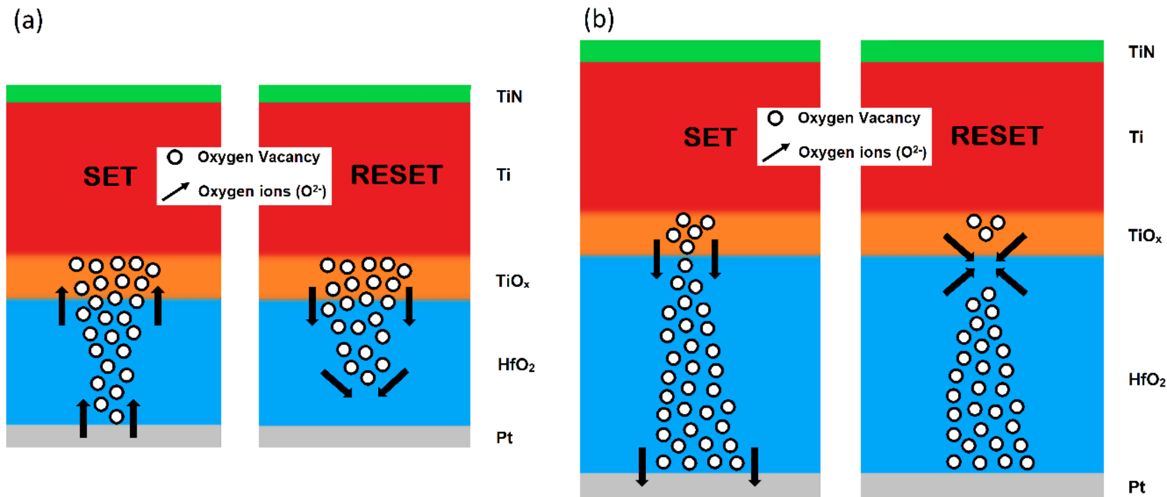

Fig. 11. Schematics of the resistive switching mechanisms for the TiN/Ti/HfO_2/Pt with HfO_2 thick layers of 8.5 nm (a) and 14 nm (b). Cited from [5] https://doi.org/10.3390/electronics11030479

4. Error balances

At our calculations, we have used the ALD cycle numbers and SE thickness values for films. The thickness values obtained from XRR are systematically lower than the SE values. The confronting results of ellipsometry and XRR measurements are due to a fact that using ellipsometry we take a possible SiO_2 natural oxide layer into account as a part of deposited film on Si substrate (refractive indices about 1.45, 1.9 and 4, correspondingly) while for XRR the film thickness is achieved without SiO_2 component due to high density of the HfO_2 material (10.14 g/cm^3) against the nearly identical density values for Si substrates (2.33 g/cm^3) and SiO_2 film (2.20 g/cm^3 for amorphous silica). Table presents the film thickness values obtained using XRR and SE for films at two growth temperatures – 200 and 300 °C.

Table 1. ALD HfO_2 film thicknesses obtained from XRR and ellipsometry (model with $k = {}^{1}/_{\lambda^2}$ for absorption index dispersion)

Growth temperature, °C	ALD cycles	*d*, nm (XRR)	*d*, nm (SE)
200	55	5.4	9.2
	110	11.4	13.8
	220	24.0	26.4
	500	46.5	51.4
300	55	4.4	8.8
	110	9.9	12.9
	220	23.0	26.0
	500	44.3	47.8

We cannot comment on the error components for X-ray reflectivity measurements of the thinner samples with poorly defined structure. However, XRR does not demonstrate the fall of material density at lower thicknesses at the same amount as ellipsometry does. Still, the quality of the XRR modelling is also somewhat improved if we define the lower density sublayer in contact with surface.

The ellipsometric modelling using the fixed film thickness from X-ray reflectivity would result in the refractive indices over 2.1 for most of 500 cycles samples at 633 nm. For comparison, we tried to correct the refractive index obtained using XRR thicknesses as

$$n' = n_{XRR} \frac{d_{XRR}}{d_{XRR}+1.5} \quad (5)$$

taking 1.5 nm for the estimated SiO_2 natural oxide thickness. Here, d_{XRR} is obtained from X-ray reflectivity and n_{XRR} from ellipsometric modelling with fixed film thickness d_{XRR}. In this case, all the obtained refractive indices for 500 cycle samples remained below 2.1 value. Applying the XRR thickness values to SE data for thinner films results in refractive index about 2.1 for them, moving after correction into 1.8 range (not shown). The correct silicon oxide thickness after the deposition process is not known.

By the same reason, we are aware that the real refractive index of our thin films is somewhat higher and their thickness somewhat lower than the data obtained from SE calculations. Therefore, the particular local refractive index values from our calculations may be taken as guesstimates, though the direction of the physical processes is seen.

5. Conclusions

Thin films deposited using ALD process and TEMAH in our deposition conditions occur to possess quite inhomogeneous nature at the first stage of growth. This factor clearly influences the refractive index values obtained using ellipsometry and in lesser amount the densities obtained using X-ray reflectivity. However, if we have success looking for a suitable model to describe the behaviour of material mean refractive index over a range of film thicknesses, we can perform the calculations and then find the approximate profile of material refractive index inside the film. In our case, the result would be refractive index rising for first 15 to 25 nm of the film growth depending on temperature.

Modelling the thin films with undefined structure creates problems in choosing the correct dispersion model for SE. We see that the character of the power function used for absorption index in the model may have a profound influence on the obtained absorption values though the fit quality does not change much. The higher powers are preferable for HfO_2 films where the crystallization takes place.

The resistive switching in HfO_2 thin films demonstrates the influence of switching behaviour on film thickness. While the 8.5 nm thick HfO_2 films showed counter-clockwise behaviour, the thicker films (14 nm) displayed a clockwise resistive switching effect. This influence was also demonstrated by other devices with the same layer disposition and fabrication process but inverted bottom and top electrodes, which showed the same thickness-dependence on resistive switching polarity. A revision of previous literature suggests that this polarity change is due to the conductive filament breaking at different interfaces. Several mechanisms could be behind this: (i) current overshoot due to parasitic capacitances discharge, (ii) the relatively thinner Ti cap for the thicker sample, which prevents the formation of enough oxygen vacancies near the Ti/HfO_2 interface, (iii) the change in material density in this metal-insulator interface and (iv) competition between CW and CCW RS, as well as URS. We propose that the change of material density together with its structure and defectivity may be a reason for such behaviour of atomic layer deposited HfO_2.

Acknowledgement

The research was funded by the Estonian Research Council (grants PRG753 "Resistive switching in artificially designed materials for data processing" and PSG448 "Formation and stabilization of high-density hard phases of optical materials in thin-film structures") and by the EU Commission through the European Regional Development Fund under project TK141 "Advanced materials and high-technology devices for sustainable energetics, sensorics and nanoelectronics".

References

[1] S. Shestaeva, A. Bingel, P. Munzert, L. Ghazaryan, Ch. Patzig, A. Tünnermann, and A. Szeghalmi, “Mechanical, structural, and optical properties of PEALD metallic oxides for optical applications“, *Appl. Opt.*, vol. 56, no. 4, pp. C47-59, 2017.

[2] G. Abromavičius, S. Kičas, R. Buzelis, “High temperature annealing effects on spectral, microstructural and laser damage resistance properties of sputtered HfO_2 and HfO_2-SiO_2 mixture-based UV mirrors“, *Opt. Mat.,* vol. 95, 109245 (7 p.), 2019.

[3] S.-J. Jeong, Y. Gu, J. Heo, J. Yang, C.-S. Lee, M.-H. Lee, Y. Lee, H. Kim, S. Park, S. Hwang, “Thickness scaling of atomic-layer-deposited HfO_2 films and their application to wafer-scale graphene tunnelling transistors“, *Scient. Reports*, vol. 6, 20907 (12 p.), 2016.

[4] A. Rodríguez Fernández, "Analysis and Modeling of Filamentary Conduction in HfO_2-Based Structures", Doctoral Thesis. Universitat Autònoma de Barcelona. June 2018.

[5] G. Vinuesa, H. García, M. B. González, K. Kalam, M. Zabala, A. Tarre, K. Kukli, A. Tamm, F. Campabadal, J. Jiménez, H. Castán, S. Dueñas, "Effect of Dielectric Thickness on Resistive Switching Polarity in TiN/Ti/HfO_2/Pt Stacks", *Electronics,* vol. 11, no. 3, 479 (9 p.), 2022.

[6] T. S. Böscke, J. Müller, D. Bräuhaus, U. Schröder, U. Böttger, "Ferroelectricity in hafnium oxide thin films", *Appl. Phys. Lett.,* vol. 99, 102903 (3 p.), 2011.

[7] M. F. Al-Kuhaili, S. M. A. Durrani, E. E. Khawaja, "Characterization of hafnium oxide thin films prepared by electron beam evaporation", *J. Phys. D: Appl. Phys.,* vol. 37, pp. 1254-61, 2004.

[8] K. Kukli, M. Ritala, T. Sajavaara, J. Keinonen, M. Leskelä, "Atomic Layer Deposition of Hafnium Dioxide Films from Hafnium Tetrakis(ethylmethylamide) and Water", *Chem. Vap. Depos.,* vol. 8 no. 5 pp. 199-204, 2002.

[9] S. Y. Lee, H. K. Kim, J. H. Lee, I-H. Yu, J-H. Lee, Ch. S. Hwang, "Effects of O_3 and H_2O as oxygen sources on the atomic layer deposition of HfO_2 gate dielectrics at different deposition temperatures", *J. Mater. Chem. C,* vol. 2, pp. 2058-68, 2014.

[10] K.-M. Kim, J. S. Jang, S.-G. Yoon, J.-Y. Yun, N.-K. Chung, "Structural, Optical and Electrical Properties of HfO_2 Thin Films Deposited at Low-Temperature Using Plasma-Enhanced Atomic Layer Deposition", *Materials* vol. 13, no. 9, 2008 (10 p.), 2020.

[11] B.-Y. Tsui, H.-W. Chang, "Formation of interfacial layer during reactive sputtering of hafnium oxide", *J. Appl. Phys.,* vol. 93, no. 12, pp. 10119-24, 2003.

[12] D. Franta, I. Ohlídal, D. Nečas, F. Vižďa, O. Caha, M. Hasoň, P. Pokorný, "Optical characterization of HfO_2 thin films", *Thin Solid Films*, vol. 519 no. 18, pp. 6085-91, 2011.

[13] E. Hildebrandt, J. Kurian, M. M. Müller, Th. Schroeder, H.-J. Kleebe, L. Alff, "Controlled oxygen vacancy induced p-type conductivity in HfO_{2-x} thin films", *Appl. Phys. Lett.,* vol. 99, 112902 (3 p.), 2011.

[14] E. S. Field, D. E. Kletecka, "Impact of contamination and aging effects on the long-term laser damage resistance of SiO_2/HfO_2/TiO_2 high reflection coatings for 1054 nm", *Opt. Eng.,* vol. 58, 105105 (5 p.), 2019.

[15] X. Nie, F. Ma, D. Ma, K. Xu, "Growth mode evolution of hafnium oxide by atomic layer deposition", *J. Vac. Sc. Technol. A*, vol. 32, 01A109 (5 p.), 2014.

[16] O. Stenzel, S. Wilbrandt, M. Schürmann, N. Kaiser, H. Ehlers, M. Mende, D. Ristau, S. Bruns, M. Vergöhl, M. Stolze, M. Held, H. Niederwald, Th. Koch, W. Riggers, P. Burdack, G. Mark, R. Schäfer, S. Mewes, M. Bischoff, M. Arntzen, F. Eisenkrämer, M. Lappschies, S. Jakobs, S. Koch, B. Baumgarten, A. Tünnermann, "Mixed oxide coatings for optics", *Appl. Opt.*, vol. 50, no. 9, pp. C69-74, 2011.

[17] M. Jerman, Zh. Qiao, D. Mergel, "Refractive index of thin films of SiO_2, ZrO_2, and HfO_2 as a function of the films' mass density", *Appl. Opt.,* vol. 44, no. 15, pp. 3006-12, 2005.

[18] M. Alvisi, S. Scaglione, S. Martelli, A. Rizzo, L. Vasanelli, "Structural and optical modification in hafnium oxide thin films related to the momentum parameter transferred by ion beam assistance", *Thin Solid Films*, vol. 354, no. 1-2, pp. 19-23, 1999.

[19] D. Franta, D. Nečas, I. Ohlídal, "Universal dispersion model for characterization of optical thin films over a wide spectral range: application to hafnia", *Appl. Opt.*, vol. 54, no. 31, pp. 9108-19, 2015.

[20] R. Waser, "Redox-Based Resistive Switching Memories", *Journal of Nanoscience and Nanotechnology,* vol. 12, no. 10, pp. 7628-40, 2012.

[21] A. C. Jasmin, "Filamentary model in resistive switching materials", *AIP Conference Proceedings*, vol. 1901, 060004 (5 p.), 2017.

[22] D. Ielmini, "Resistive switching memories based on metal oxides: mechanisms, reliability and scaling", *Semiconductor Science and Technology*, vol. 31, 063002 (25 p.), 2016.

[23] L. Goux, X. P. Wang, Y. Y. Chen, L. Pantisano, N. Jossart, B. Govoreanu, J. A. Kittl, M. Jurczak, L. Altimime, D. J. Wouters, "Roles and Effects of TiN and Pt Electrodes in Resistive-Switching HfO_2 Systems", *Electrochem. Solid State Lett.,* vol. 14, no. 6, pp. H244–6, 2011.

[24] C. Giovinazzo, J. Sandrini, E. Shahrabi, O. T. Celik, Y. Leblebici, C. Ricciardi, "Analog Control of Retainable Resistance Multistates in HfO_2 Resistive-Switching Random Access Memories (ReRAMs)", *ACS Appl. Electron. Mater.*, vol. 1, no. 6, pp. 900–909, 2019.

[25] S. Brivio, J. Frascaroli, S. Spiga, "Role of metal-oxide interfaces in the multiple resistance switching regimes of Pt/HfO_2/TiN devices", *Appl. Phys. Lett.*, vol. 107, 023504 (6 p.), 2015.

[26] M. Otsus, J. Merisalu, A. Tarre, A.-L. Peikolainen, J. Kozlova, K. Kukli, A. Tamm, "Bipolar Resistive Switching in Hafnium Oxide-Based Nanostructures with and without Nickel Nanoparticles", *Electronics*, vol. 11, no. 18, 2963 (18 p.), 2022.

[27] L. Goux, Y.-Y. Chen, L. Pantisano, X.-P. Wang, G. Groeseneken, M. Jurczak, D. J. Wouters, "On the Gradual Unipolar and Bipolar Resistive Switching of TiN\HfO_2\Pt Memory Systems", *Electrochem. Solid State Lett.*, vol. 13, no. 6, pp. G54–6, 2010.

[28] I. Valov, "Interfacial interactions and their impact on redox-based resistive switching memories (ReRAMs)", *Semiconductor Science and Technology*, vol. 32, 093006 (20 p.), 2017.

Authors' biographies

Aarne Kasikov is a researcher in the University of Tartu (UT). He was born in 1957, MSc. from the UT 1995, PhD (UT) 2010. He has dealt with vacuum evaporation, production of optical coatings, laser-induced damage in optical coatings, and measurement of the optical parameters of thin films using spectrophotometry and ellipsometry. Special interests – characterization of inhomogeneous films with changing refractive index through material, history.

Aivar Tarre was born at Pärnu County, Estonia, in 1972. He obtained the MSc degree in the field of Applied Physics from the University of Tartu at 1999. Until now he works as an engineer in the Institute of Physics, University of Tartu. His main research interests are atomic layer deposition of thin oxide films and their post-deposition characterization.

Guillermo Vinuesa is a doctor of physics and Adjunct Professor at the Department of Electronics of the University of Valladolid. His research is dedicated to the electrical characterization of thin films, dealing with the conduction mechanisms and underlying physics behind the resistive switching effect, a property that allows certain materials to change their resistance by applying an electric field. He has several scientific contributions in JCR-indexed journals as well as to international conferences and has been member of several I+D projects focused on resistive switching devices. He collaborates regularly with the University of Tartu in Estonia and the IHP-Leibniz-Institute for Innovative Microelectronics in Germany, as well as with the University of Granada and the Barcelona Microelectronics Institute in Spain (IMB-CNM/CSIC).

Received 11 May 2023